J. Fluid Mech. (1983), vol. 133, pp. 161–177
Printed in Great Britain

Fluid-property effects on flow-generated waves on a compliant surface

By R. J. HANSEN
Fluid Dynamics Branch, Naval Research Laboratory, Washington, D.C., 20375

AND D. L. HUNSTON
Polymer Science and Standards Division, National Bureau of Standards, Washington, D.C., 20234

(Received 28 April 1982 and in revised form 3 February 1983)

An experimental study of the influence of liquid viscosity and viscoelasticity on flow-generated waves on a compliant surface has been conducted in a rotating-disk geometry. Over the entire range of liquid properties studied, each test gave a well-defined critical onset flow velocity above which waves were present and below which no waves were observed. This onset velocity increased with increasing fluid viscosity, and for sufficiently high viscosities the onset occurred when the flow on the disk was laminar rather than turbulent. The effects of liquid viscoelasticity were examined in the turbulent flow using dilute solutions of high-molecular-weight polymers. This type of viscoelasticity had little influence on the onset flow velocity in these circumstances, but did make the wave structure on the surface more regular in appearance than when the liquid was Newtonian. In all cases the wave structure produced a dramatic increase in drag similar to that expected for a rough surface. For the viscoelastic fluid, however, the increase in drag was much less than for a viscous fluid of the same viscosity.

1. Introduction

It is well known that the turbulent flow of water across a compliant surface can produce a nearly stationary wave-like deformation in that surface. In recent years experimental studies (Hansen & Hunston 1974, 1976; Brown 1977; Hansen *et al.* 1979; Hansen *et al.* 1980) have shown that for a given compliant surface there is a critical flow velocity above which the waves are present. These studies have established the wavelengths and propagation velocities for these waves as well as defining a relationship between the onset flow velocity and the shear modulus of the compliant material. None of these studies, however, have considered the influence of the properties of the fluid.

The purpose of the present investigation has been to determine the effect of liquid viscosity and certain types of liquid viscoelasticity on this hydroelastic instability phenomenon. Particular attention has been given to the onset conditions for the wave structure, its appearance above the onset velocity, and its influence on skin-friction drag. The rotating-disk geometry has been utilized in the study because it requires suitably small amounts of test liquids. (Fluid-property studies are impractical in a water tunnel because of the time and expense associated with changing the test liquids.) Recently reported experiments (Hansen *et al.* 1980) have established that the features of the wave structure are the same in the rotating-disk and flat-plate

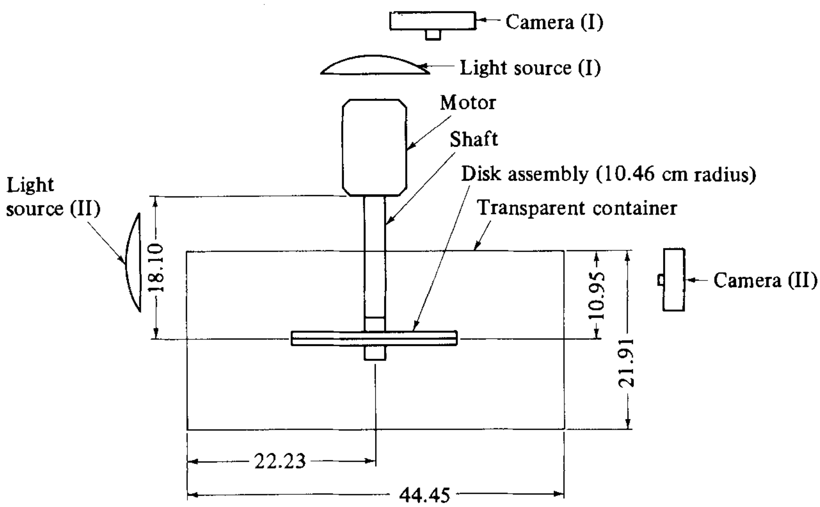

FIGURE 1. Schematic drawing of the larger (20.92 cm diameter) rotating-disk apparatus (Hansen & Hunston 1974).

geometries. In both cases the wave crests are oriented at approximately 90° to the flow direction (as seen by an observer on the surface), and the wave propagation velocity in this reference frame is orders of magnitude smaller than the freestream fluid velocity. Perhaps even more significant is the fact that the measured freestream fluid velocity for the onset of the phenomenon is within 10 % in the two geometries for any given shear modulus of the compliant material.

2. Experimental apparatus and procedures

The experimental apparatus and procedures employed were in most respects identical to those utilized in the authors' earlier rotating-disk experiments with water (Hansen & Hunston 1974). The same two rotating-disk systems were employed. In these two geometrically similar systems the disk diameters were 10.16 and 20.92 cm. The larger system is shown schematically in figure 1. The transparent container was sufficiently large in each case that the disk rotated in an essentially infinite medium. In all cases the experiments were conducted in a constant-temperature environment with air and liquid temperatures being 22 ± 1 °C.

As in the earlier experiments the compliant surfaces were elastomers made with polyvinyl chloride (PVC) plastisols. These elastomers were prepared with 10, 15 and 20 % by weight of PVC resin, a plasticizer (DOP or di-2-ethyl hexyl phthalate), and a dibutyl maleate stabilizer. The associated shear moduli were measured and reported in the initial rotating-disk study (Hansen & Hunston 1974), although some batch-to-batch variations in modulus are expected since the thermal history during sample preparation could not be completely controlled. The measurements reported in that study also established that the elastomers approximate perfectly elastic solids over the ranges of frequency and strain amplitude believed to be associated with the hydroelastic instability phenomenon. The compliant material was applied to the disk in the molten state by pouring it into the recessed regions of the two halves of the rotating-disk structure while they were removed from the shaft (figure 2). After cooling, the disk structure was reassembled.

To study the influence of liquid viscosity on the flow-generated waves, water–gly-

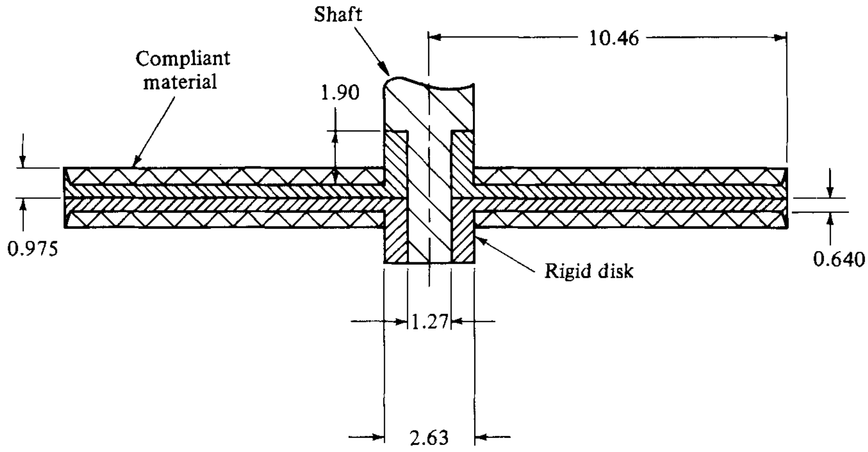

FIGURE 2. Schematic drawing of the larger (20.92 cm diameter) disk assembly (Hansen & Hunston 1974).

Test-condition designation†	Disk diameter	Glycerol content (% by weight)	Fluid viscosity	Resin content (% by weight)	Shear modulus of coating
1, 1W	10.16 cm	25 %	2.06 cP	10 %	5250 dyn/cm^2
2, 2W	10.16 cm	50 %	5.23 cP	10 %	5250 dyn/cm^2
3, 3W	10.16 cm	50 %	5.23 cP	15 %	22300 dyn/cm^2
4, 4W	10.16 cm	50 %	5.23 cP	20 %	58200 dyn/cm^2
5, 5W	10.16 cm	75 %	34.0 cP	10 %	5250 dyn/cm^2
6	10.16 cm	25 %	2.06 cP	solid disk	—
7	10.16 cm	50 %	5.23 cP	solid disk	—
8	10.16 cm	50 %	5.23 cP	solid disk	—
9	10.16 cm	50 %	5.23 cP	solid disk	—
10	10.16 cm	75 %	34.0 cP	solid disk	—
11, 11W	20.92 cm	25 %	1.99 cP	10 %	5250 dyn/cm^2
12, 12W	20.92 cm	50 %	5.71 cP	10 %	5250 dyn/cm^2
13, 13W	20.92 cm	75 %	31.0 cP	10 %	5250 dyn/cm^2
14	20.92 cm	25 %	1.99 cP	solid disk	—
15	20.92 cm	50 %	5.71 cP	solid disk	—
16	20.92 cm	75 %	31.0 cP	solid disk	—

† 'W' designates tests with equivalent conditions but using water rather than glycerol solution

TABLE 1. Experimental conditions: viscous fluid

cerol solutions were utilized. These solutions are Newtonian and show no measurable viscoelasticity. Nominal concentrations by weight of glycerol in water of 25, 50, and 75 % were employed. Since glycerol tends to absorb water, however, the actual viscosity of each solution was measured rather than relying on published values. The viscosities were measured at 22.00 ± 0.01 °C using a Cannon 4-bulb viscometer.

Table 1 gives a summary of the test conditions used in the flow experiments related to viscosity effects. In most cases a number of experiments were performed at each set of test conditions and average values were obtained. Moreover, for each test condition in which a coating was used, two experimental setups were employed: one containing the glycerol solution and the other containing pure water (designated in table 1 with 'W'). In this way the onset velocity in water and glycerol solution could

Test-condition designation†	Disk diameter	Polymer concentration	Polymer type	Resin content (% by weight)	Shear modulus of coating
17–24	10.16 cm	0, 2.5, 5, 10, 25, 50, 100, 200	P250	Solid disk	—
25–30	10.16 cm	0, 1.25, 2.5, 5, 10, 25, 50	AP30	Solid disk	—
32,32W	10.16 cm	100	P250	15%	22300 dyn/cm^2
33,33W	10.16 cm	100	P250	20%	58200 dyn/cm^2
34	10.16 cm	100	P250	Solid disk	—
35,35W	20.92 cm	25	AP30	15%	22300 dyn/cm^2
36	20.92 cm	25	AP30	Solid disk	—

† 'W' designates test with equivalent conditions but using water rather than polymer solution

TABLE 2. Experimental conditions: viscoelastic fluid

be obtained in sequence for the same coating with the same thermal and preparative history.

A complete examination of the influence of all types of fluid viscoelasticity is a very complex undertaking and was not attempted in the present study. One aspect of solution viscoelasticity that is of particular interest, however, was addressed. Very dilute solutions of high-molecular-weight polymers are known to exhibit a number of unusual effects such as reduced heat transfer, altered streamline patterns near stagnation points, inhibited cavitation inception, reduced turbulent drag, high elongational viscosity, and altered jet break-up characteristics (Ting & Hunston 1977; Metzner & Metzner 1970; Little *et al.* 1975). It has been suggested that most or all of these properties reflect solution viscoelasticity. Moreover, more concentrated solutions of these polymers show other characteristics, such as recoil, that are often associated with fluid elasticity. As a result it was of interest to examine the influence of this type of viscoelasticity on the flow-generated wave structures.

Two different polymers were tested: Cynamer-P250, which is a polyacrylamide made by American Cyanamide Company, and Separan AP-30, which is a synthetic polymer (probably based on polyacrylic acid) manufactured by the Dow Chemical Company. The test conditions employed with these viscoelastic fluids are listed in table 2. As in table 1, a number of experiments were performed at each set of test conditions so average values could be obtained. Moreover, just prior to each test utilizing a coated disk, a companion experiment was also performed in water using the same disk so that an accurate comparison of onset velocities could be made. (These tests in water are designated in table 1 with 'W'.)

In order to determine the best value of polymer concentration to be used in the coated disk experiments, a series of tests were performed using a solid disk with various polymer concentrations. Below a certain critical velocity the behaviour of the polymer solution was identical to that for water. At higher velocities the drag was lower in the polymer solution than in water. The percent reduction in drag D can be defined as

$$D = 100\frac{(C_{\mathrm{M}})_{\mathrm{W}} - (C_{\mathrm{M}})_{\mathrm{S}}}{(C_{\mathrm{M}})_{\mathrm{W}}}, \tag{1}$$

where

$$C_{\mathrm{M}} = \frac{2T}{\rho\omega^2 R^5}, \tag{2}$$

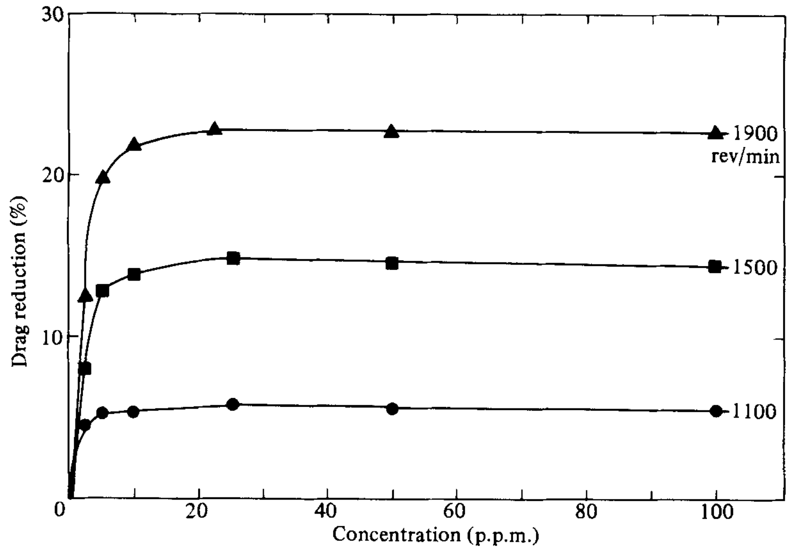

FIGURE 3. Percent reduction in drag *vs.* polymer concentration for P250 at 3 different rotational speeds (10.16 cm diameter disk): ▲, 1900 rev/min; ■ 1500 rev/min; ●, 1100 rev/min.

and T denotes torque, ρ the liquid density, ω the rotational speed in rad/sec, and R the disk radius. The subscripts W and S identify the test liquid as water or the polymer solution respectively. Above the onset point, D increases with increasing velocity. The concentration dependence of D is shown in figure 3, which gives the data for P250 at 3 different rotational speeds. The results for AP-30 are similar, although somewhat lower concentrations are required to produce the same effect. As can be seen from this figure, there is a very rapid rise in D at low concentrations followed by a long plateau region where D is relatively constant.

All of the results for concentration-dependence tests were obtained in short-duration experiments because the polymer degrades slowly when exposed to high shear for significant periods of time. For this same reason the coated-disk experiments were conducted using a polymer concentration that fell in the centre of the plateau region. In this way if the actual concentration of the active molecular weight species was reduced somewhat by degradation during the course of the experiment, the effects on the flow would be minimal. The concentrations selected for these tests were 100 parts per million by weight (p.p.m.) for P250 and 25 p.p.m. for AP-30.

The viscosities of the polymer solutions were also measured with the 4-bulb viscometer. A very modest decrease in solution viscosity, of the order of 10 %, was noted between the lowest and highest shear rates imposed by the viscometer (30 and 300 s^{-1} respectively). As will become apparent from the experimental results reported below with water–glycerol solutions, viscosity variations of this magnitude have a small effect on the rotating-disk experiments.

Since the drag-reducing phenomenon in the polymer solutions occurs only in turbulent flow, all of the experiments were restricted to this regime. Moreover, attention was limited to circumstances where the onset velocity for reduced drag was less than that for the wave structure. In these circumstances the influence of liquid viscoelasticity could be ascertained apart from such complicating factors as the influence of the wave structure on the onset velocity for drag reduction.

3. Experimental results

In discussing the experimental results, the influence of fluid properties on the torque coefficient *vs.* rotational Reynolds number relationship will first be examined for the flows over flexible surfaces. The relationship of the onset of the wave structure to fluid viscosity and viscoelasticity is then presented. Finally, the results of visual studies of the flow-generated wave structure are given.

3.1. *Torque coefficient vs. rotational Reynolds number*

The relationship of torque coefficient C_M to rotational Reynolds number N has been determined as a function of fluid viscosity for the conditions listed in table 1, where

$$N = \frac{R^2\omega}{\nu}, \tag{3}$$

and ν is the kinematic viscosity of the fluid. Table 1 shows that, in the course of the experiments reported here, both the fluid kinematic viscosity and the shear modulus of the compliant material have been varied over a range of more than one order of magnitude. The values listed for the shear moduli were obtained from the results published previously (Hansen & Hunston 1974). However, as indicated earlier, the actual values may be expected to vary slightly from the listed moduli since the thermal history during sample preparation is never exactly the same.

The experimental results are shown in figure 4 for the smaller-diameter disk and figure 5 for the larger one. Also shown in these figures are the result obtained with rigid disks, the theoretically predicted C_M *vs.* N curve for laminar flow on the disk (dashed line), and the corresponding result for turbulent flow on the disk (solid line) (Dorfman 1963). A number of observations may be made from these figures. First, the results measured with the rigid disks agree with the previously reported correlations between C_M and N within the experimental uncertainty of $\pm 7\,\%$ in C_M and $\pm 2\,\%$ in N. Secondly, the skin-friction drag is unaltered by surface compliance below a critical onset value of N that depends on both the fluid viscosity and the coating shear modulus. In every case, however, the drag is increased above this onset condition. Thirdly, this onset condition, which corresponds to the development of a wave structure in the compliant material–liquid interface, can occur in the laminar-flow regime if the solvent viscosity is sufficiently large. This is the case in the two highest-viscosity cases studied with the smaller disk (experiments 2 and 5) and the highest-viscosity experiments conducted with the larger disk (experiment 13). Fourthly, as N increases above the onset value, C_M reaches a maximum and is thereafter constant or decreases slightly. This behaviour is evident in experiments 1, 2 and 5 with the smaller disk (10 % by weight resin and 25, 50 and 75 % by weight glycerol in the solution). In the remaining experiments it was not possible to achieve sufficiently high torques with the apparatus used here to see this effect. Fifthly, in cases where no surface waves are present, the surface compliance appears to have little or no effect on the Reynolds number at which the laminar-to-turbulent transition occurs. For example, the value of N at transition is approximately 0.75×10^5 for the smaller rigid disk in a 50 % glycerol solution compared with approximately 0.55×10^5 for a disk with a 20 % by weight coating in the same solution.

The influence of fluid viscoelasticity is illustrated in figure 6, where the torque coefficients $(C_M)_S$ and $(C_N)_W$, normalized by the equivalent torque coefficient for a solid disk in water C_{MR}, is plotted as a function of the rotational Reynolds number for solid and coated (15 %) disks in water and in a 100 p.p.m. solution of P250

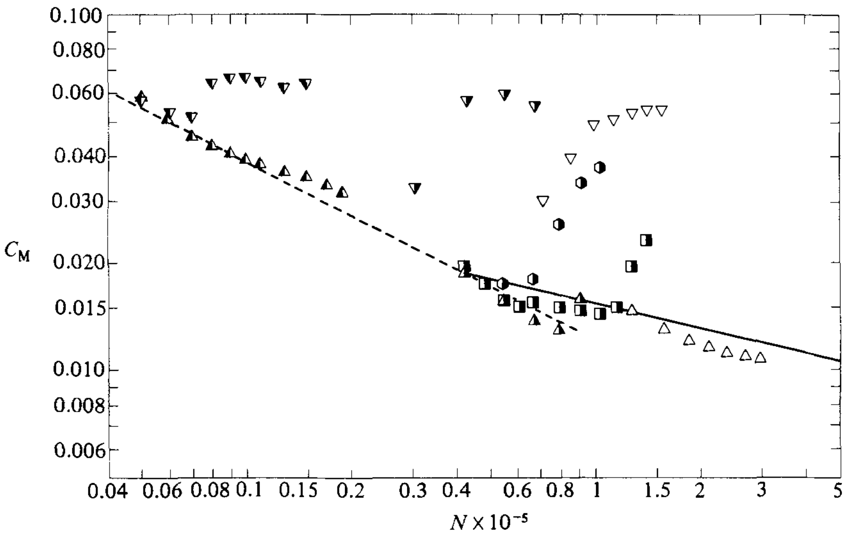

FIGURE 4. Liquid-viscosity effects on the torque-coefficient–rotational-Reynolds-number relationship (10.16 cm diameter disk): △, solid disk in 25 % glycerol solution (experiment 6); ▽, 10 % resin surface in 25 % glycerol solution (experiment 1); ▲, solid disk in 50 % glycerol solution (experiment 7); ▼, 10 % resin surface in 50 % glycerol solution (experiment 2); ◑, 15 % resin surface in 50 % glycerol solution (experiment 3); ◨, 20 % resin surface in 50 % glycerol solution (experiment 4); ◭, solid disk in 75 % glycerol solution (experiment 10); ▼, 10 % resin surface in 75 % glycerol solution (experiment 5).

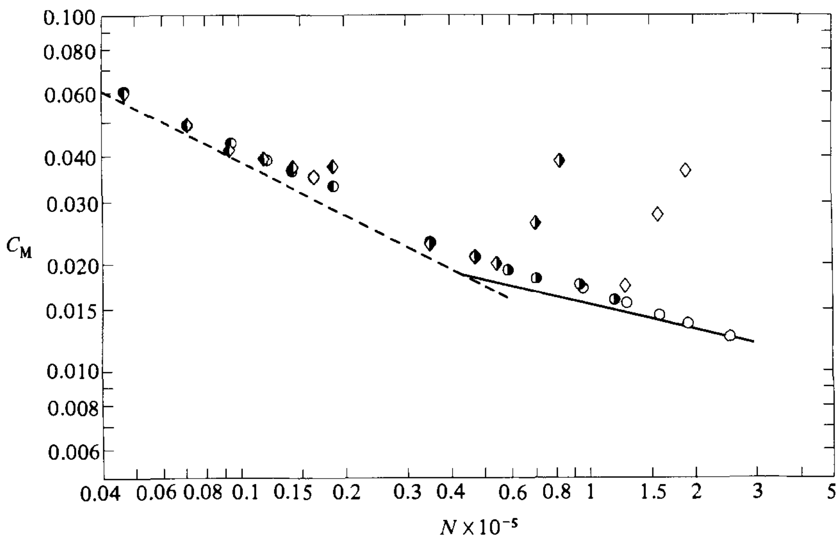

FIGURE 5. Liquid-viscosity effects on the torque-coefficient–rotational-Reynolds-number relationship (20.92 cm diameter disk): ○, solid disk in 25 % glycerol solution (experiment 14); ◇, 10 % resin surface in 25 % glycerol solution (experiment 11); ◑, solid disk in 50 % glycerol solution (experiment 15); ◈, 10 % resin surface in 50 % glycerol solution (experiment 12); ◐, solid disk in 75 % glycerol solution (experiment 16); ◈, 10 % resin surface in 75 % glycerol solution (experiment 13).

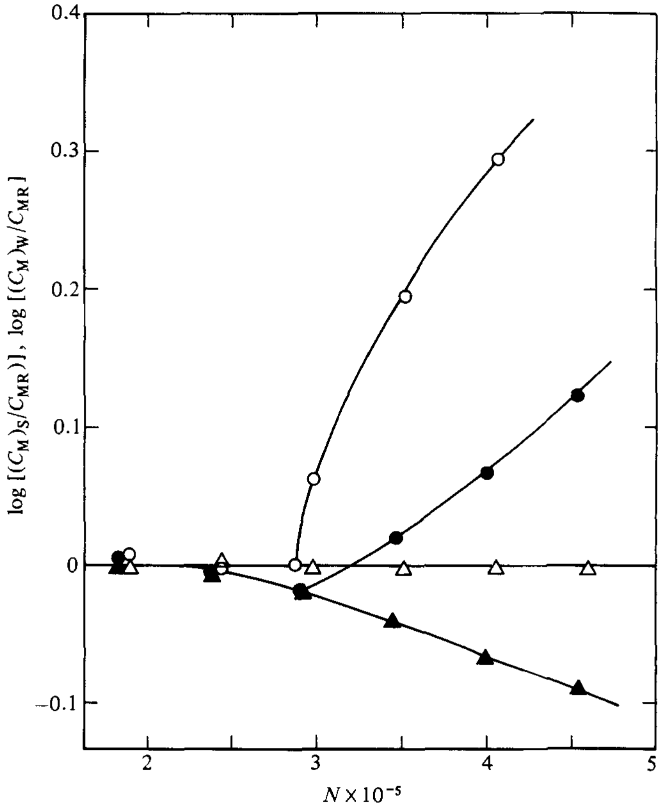

FIGURE 6. Liquid-viscoelasticity effects on the normalized torque-coefficient–rotational-Reynolds-number relationship (10.16 cm diameter disk): △, solid disk in water (experiment 17); ▲, solid disk in aqueous polymer solution (experiment 34); ○, 15 % resin surface in water (experiment 32W); ●, 15 % resin surface in polymer solution (experiment 32).

(experiments 32, 34). Since the solid-disk/water system is used as a reference, the data for these experiments fall along a horizontal line at $C_M/C_{MR} = 1$, or $\log(C_M/C_{MR}) = 0$. Deviations above and below this line therefore represent increases or decreases in drag. As expected the polymer-solution–solid-disk results are identical with those for the water–solid-disk system up to a critical Reynolds number ($N_{DR} = 2.2 \times 10^5$). Above this onset point, the drag in the polymer solution is less than that in water, with the magnitude of the reduction in drag increasing with increasing N. The data for the coated disk in water also give the expected result. The coating has no effect up to the onset point for the wave structure ($N = 2.9 \times 10^5$). Above this onset point, there is a dramatic increase in drag. When the coated disk is tested in the polymer solution, effects of both the solution and coating can be seen. The onset points remain unchanged, and thus the data fall along the solid-disk/water line up to the onset of the reduced drag effect. Above this point the data fall along the solid-disk/polymer-solution curve, indicating a reduction in drag relative to the solid disk in water. Below the onset point for the wave structure, therefore, the coating has little or no effect on the normal polymer-solution mechanisms for reducing drag. Above the onset point for the wave structure, the drag increases very rapidly. The figure indicates that the drag-increasing effect of the wave structure in the coating has a much greater influence than the drag-reducing effect of the polymer. As a result, above the onset

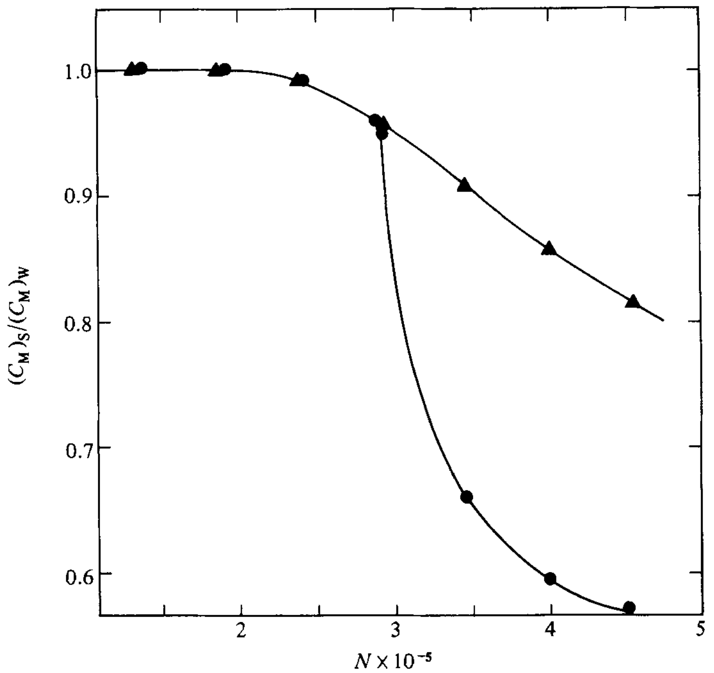

FIGURE 7. Comparison of the drag-reducing effect of liquid viscoelasticity in the presence and the absence of the wave structure (same systems as figure 6): ▲, solid disk; ●, coated disk.

point for the wave structure the drag on the coated disk in the polymer solution is in most cases significantly greater than that for the solid disk in water.

To isolate the effect of the polymer solution, however, it is also useful to consider another comparison. The drag on the solid disk in the polymer solution relative to the drag on the solid disk in water can be compared with the drag on the coated disk in the polymer solution relative to the drag on the coated disk in water. Figure 7 shows the results of a plot of $(C_M)_S/(C_M)_W$ *vs.* N for the 15 % coating and a solution containing 100 p.p.m. of P250. (Once again the subscripts S and W denote the solution and water as the test liquids.) As in the previous figure, the effect of the polymer solution is the same for coated and solid disks below the onset of the wave structure. At higher speeds, however, figure 7 shows the surprising result that the polymer solution has a much greater effect on the drag of a coated disk than on that of a solid disk. A possible explanation for this will be offered below.

3.2. *Onset conditions for the wave structure*

Previous studies (Hansen & Hunston 1974) using water have shown that the onset point for the wave structure as measured through visual observations of the disk is, within experimental uncertainty, identical with the point where the torque-coefficient–rotational-Reynolds-number curve for the coated disk departs from that for the equivalent solid disk. To determine if this is also true in the glycerol and polymer solutions, both methods were used to determine the onset points. In the first type of experiment (test conditions 1 and 1 W for example), a coated disk was first tested in water and then immediately thereafter in the glycerol or polymer solution of interest, noting in both cases the rotational speed at which the wave structure could first be observed visually. By using companion experiments on the same disk, the

Test-condition designation	Onset rotational speed in glycerol or polymer solution (rev/min)	Onset rotational speed in water (rev/min)	Ratio of onset velocity in solution to that in water	Kinematic viscosity (normalized by that of water)
1,1W,6	463	442	1.05	1.94
2,2W,7	480	423	1.13	4.64
3,3W,8	1135	938	1.21	4.64
4,4W,9	1885	1520	1.24	4.64
5,5W,10	669	442	1.51	28.4
11,11W,14	223	208	1.07	1.87
12,12W,15	259	207	1.25	5.06
13,13W,16	353	200	1.77	25.9
32,32W,34	1513	1536	0.99	1.1
33,33W,34	1021	1045	0.98	1.1
35,35W,36	467	440	1.06	1.1

TABLE 3. Onset conditions for the wave structure

fluid-property effects on onset could be determined with minimal influence of slight variations in the shear modulus of the compliant material which are present in samples of a given resin content made up at different times. In the second type of experiment (test conditions 1 and 6 for example), the rotational speeds (or values of N) at which solid and coated disk results first began to diverge in C_M *vs.* N plots (figures 4–6) were noted. As in the previous study (Hansen & Hunston 1974), the results obtained in these two ways were in good agreement, because of the cause–effect relationship between the existence of the wave structure and the increased hydrodynamic drag on a disk.

The rotational speeds and related quantities for the onset of the wave structure are tabulated in table 3. It is evident from this tabulation that the onset rotational speed (or associated flow velocity adjacent to the disk) is not significantly affected by liquid viscoelasticity, but it does increase with increasing liquid viscosity. This influence of viscosity is shown graphically in figure 8, in the form of a plot of normalized onset rotational speed ω_0/ω_{0W} *vs.* normalized kinematic viscosity ν/ν_W. Here ω_0 denotes the onset rotational speed for the wave structure, and the subscript W has been used to denote the values pertaining to water. In these terms a slight influence of resin content at a given kinematic viscosity is also observed. Note from figure 4 that the onset condition is in the laminar regime for the wave structure on the 10 % resin surface at the two higher kinematic viscosity ratios (experiments 2 and 5).

3.3. *Photographic studies of the wave structure*

Photographic records of the waves on the flexible surfaces were made with the camera and strobe light placed as shown in figure 1. The camera was opened for one flash of the strobe. As in the authors' earlier work (Hansen & Hunston 1974) this arrangement provided excellent pictures of the wave structure, although the view of a portion of the disk was blocked by the light source.

Figure 9 shows the wave structure in experiment 11 (i.e. larger disk, 25 % glycerol solution, 10 % resin content). Rotation of the disk is clockwise in each case, so that

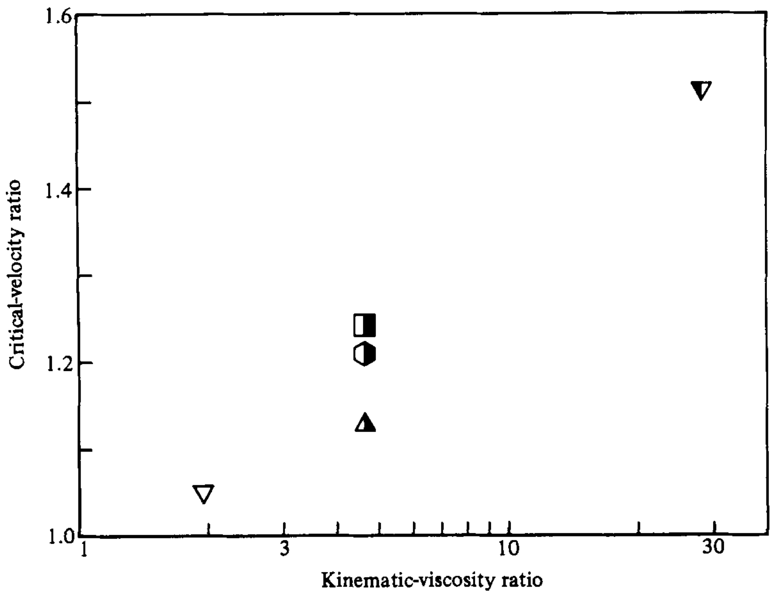

FIGURE 8. Influence of the liquid kinematic viscosity (normalized by the kinematic viscosity of water) on the onset rotational speed for the wave structure (normalized by the onset rotational speed for the same surface in water). Symbols are the same as for figure 4. The normalized critical velocity ratios are obtained by normalizing the results of experiments 1, 2, 3, 4 and 5 by those of experiments 1W, 2W, 3W, 4W and 5W, respectively.

the freestream fluid velocity in a reference frame rotating with the disk is essentially perpendicular to the wave crests. The photographs cover the rotational speed range from just above the onset of the wave structure to 1.81 times the onset value. The onset of the hydroelastic instability phenomenon occurs in the turbulent-flow regime in this case, and the appearance of the wave structure is essentially the same as that observed previously (Hansen & Hunston 1974) with water in place of the water–glycerol solution. The waves extend progressively farther inward and become more complex in their configuration with increasing flow velocity. The propagation velocity of the waves relative to the disk is negligibly small in all cases.

A wave structure of strikingly different appearance existed when the onset condition was in the laminar regime. Figure 10 shows this structure for experiment 13, for rotational velocities from 1.02 to 1.22 times the onset value. (Torque limitations in the motor turning the disk prevented observations at higher rotational speeds in this case.) The difference in the spacing between wave crests in this case and that shown in figure 9 is particularly noteworthy. At 1.02 times the onset flow velocity, for example, the average azimuthal spacing between crests is approximately 7.4° in figure 9 compared with 32° in figure 10. At 1.20 times the onset velocity this spacing is 6.9° in figure 9 and 15° in figure 10.

Figure 11 shows that the wave structure in the presence of liquid viscoelasticity differs from that exhibited in the presence of a Newtonian liquid with the onset in either the laminar- or the turbulent-flow regime. In this particular case the larger disk with a 15% by weight resin surface was rotated in an aqueous solution of AP30 at a concentration of 25 p.p.m. by weight (test condition 35). It is noted in particular that the wave crests are more regularly spaced and less complicated in shape than in either figure 9 or figure 10. This 'smoothing' effect of polymer solutions has been seen in a number of different experiments such as jet break-up and the stability of

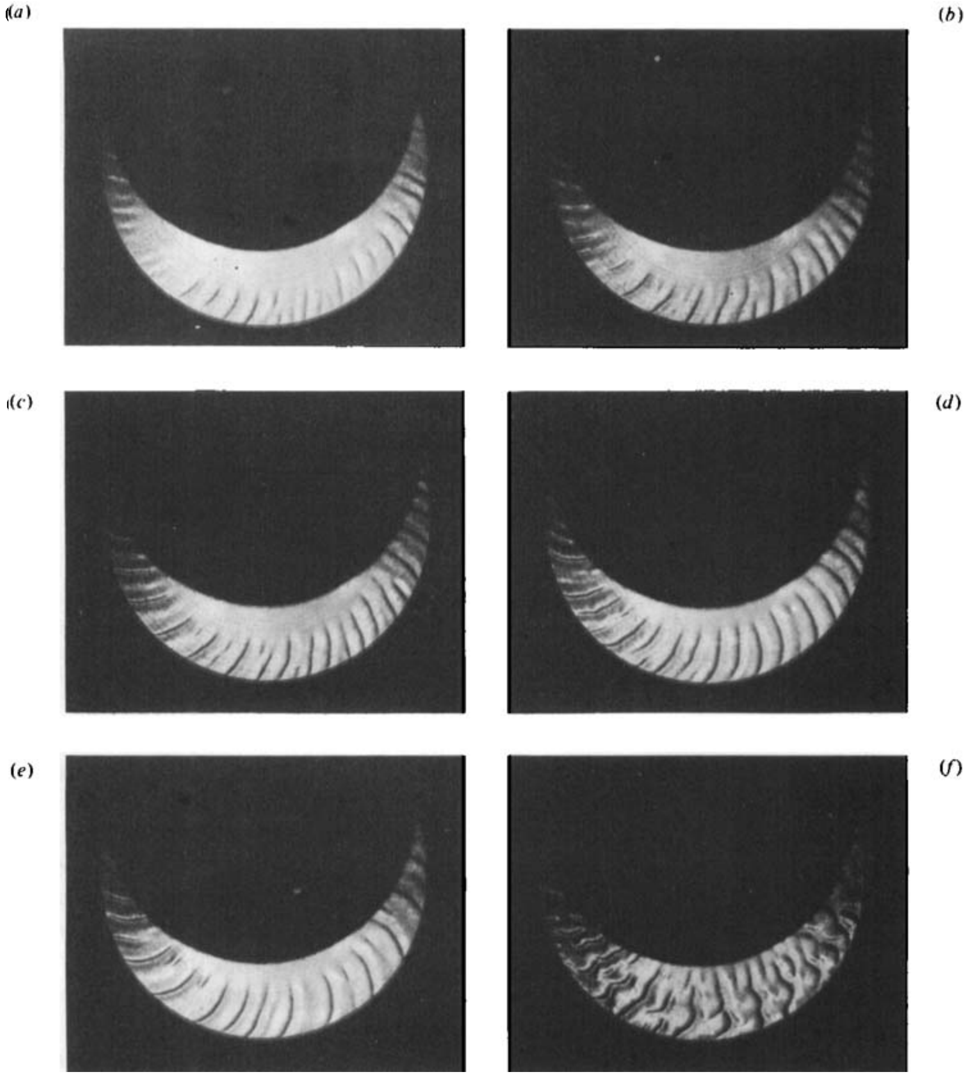

FIGURE 9. Photographs of 20.92 cm diameter disk with a 10% resin surface rotating in a 25% glycerol solution (experiment 11); onset in the turbulent regime: (*a*) 1.02 times onset velocity; (*b*) 1.06 times onset velocity; (*c*) 1.16 times onset velocity; (*d*) 1.20 times onset velocity; (*e*) 1.30 times onset velocity; (*f*) 1.81 times onset velocity.

liquid sheets (Ting & Hunston 1977). It is apparently characteristic of the influence of this type of liquid viscoelasticity on complex fluid-flow phenomena. Another feature of the wave structure shown in figure 11 is the spacing of the crests. At rotational speeds exceeding the onset value by a small amount, the azimuthal spacing between crests is less than in the fully turbulent case. At 1.06 times the onset velocity, for example, the average azimuthal spacing is 7.5° in figure 9 compared with 5.2° in figure 11.

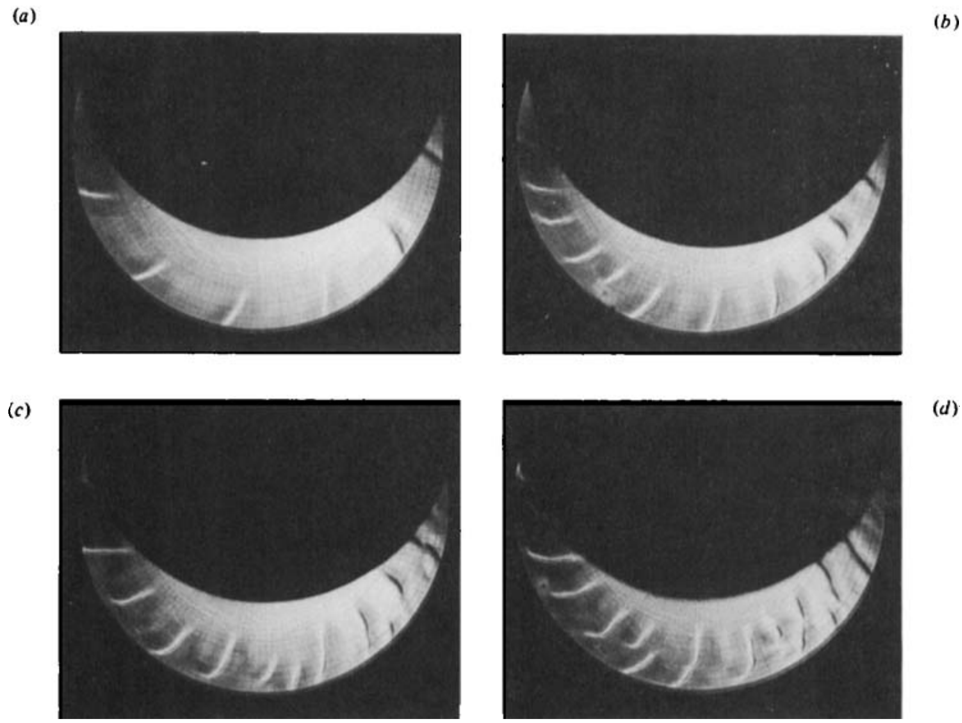

FIGURE 10. Photographs of 20.92 cm diameter disk with a 10 % resin surface rotating in a 75 % glycerol solution (experiment 13); onset in the laminar-flow regime: (*a*) 1.03 times onset velocity; (*b*) 1.06 times onset velocity; (*c*) 1.15 times onset velocity; (*d*) 1.22 times onset velocity.

4. Discussion

As has been previously noted (Hansen *et al.* 1980), the flow-generated wave structure on a compliant surface is nearly stationary, its propagation velocity relative to the rigid substrate being approximately two orders of magnitude smaller than the freestream fluid velocity. Therefore it has much the same effect on the skin-friction drag as surface roughness on a rigid disk. It alters the adjacent boundary-layer structure in such a way as to increase hydrodynamic drag. The degree of similarity between the wave-structure effects on a disk with a compliant surface and surface roughness on a rigid disk is particularly evident in experiments 1 and 2. As the rotational speed of the compliant disk was increased to substantially above the onset condition in these two cases, the value of N was in the turbulent regime, and the skin-friction coefficient rose to a maximum value and then exhibited little change with further increase in N. This is precisely the behaviour predicted theoretically and observed experimentally (Dorfman 1963) for a rigid disk with a rough surface rotating in Newtonian fluid, when the adjacent boundary-layer flow is turbulent. It is interesting to note that the C_M *vs.* N behaviour for experiment 5 is very much like that in experiments 1 and 2, although the value of N is well within what is ordinarily the laminar-flow range on the disk. The similarity suggests that, once the waves come into existence in this laminar-flow regime, they cause the transition from laminar to turbulent flow to occur. This suggestion is consistent with the well-known influence of surface roughness in promoting transition on a rigid surface.

The wave structures observed in figure 9–11 have a superficial similarity in

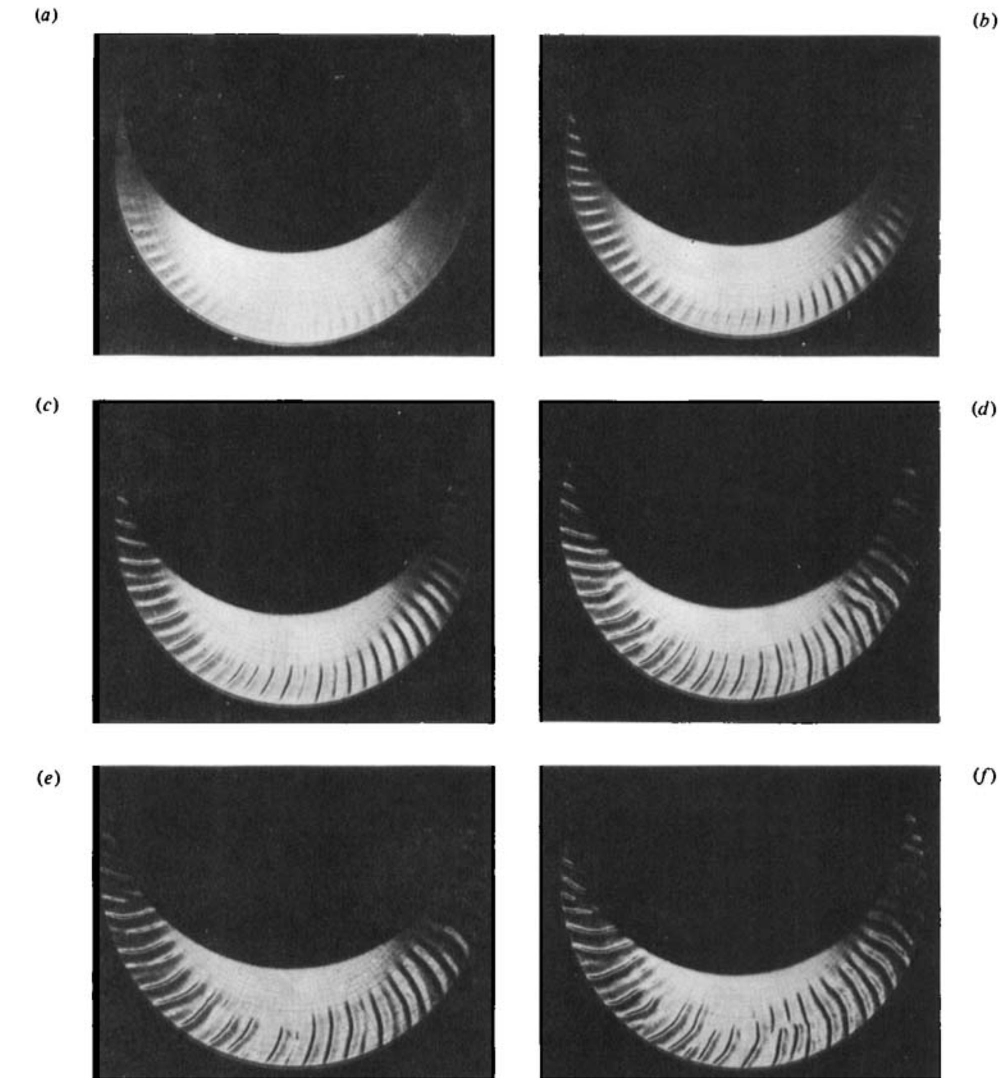

FIGURE 11. Photographs of 20.92 cm diameter disk with a 15 % resin surface rotating in a viscoelastic liquid (experiment 35); (*a*) 1.02 times onset velocity; (*b*) 1.07 times onset velocity; (*c*) 1.17 times onset velocity; (*d*) 1.20 times onset velocity; (*e*) 1.31 times onset velocity; (*f*) 1.50 times onset velocity.

appearance to the pattern visualized on a rigid disk (Gregory, Stuart & Walker 1955) with a very thin layer of kaolin. In fact the orientations as well as the origins of the two sets of patterns are entirely different from one another. This may not be immediately apparent because the famous photographs of the rigid disk were taken with *counterclockwise* rotation, whereas rotation is *clockwise* in the present investigation. In the reference frame rotating with the disk the crests of the kaolin patterns are nearly aligned with the flow direction at the edge of the boundary layer ($\zeta = z(\omega/\nu)^{\frac{1}{2}} \approx 4$) and aligned precisely with the velocity vector at $\zeta = 1.4$ (Dorfman 1963). Here ζ and z denote normalized and dimensional distances perpendicular to the plane of the disk, respectively. In the same reference frame the orientation of the wave crests on the compliant surfaces is nearly perpendicular to the flow direction at the edge of the boundary layer and exactly perpendicular to the velocity vector at ζ in the 1.4 range. In other words, the kaolin and compliant surface wave patterns are orthogonal to one another.

The causes of the kaolin patterns on a rigid disk and the compliant surface wave patterns are also entirely different. The kaolin pattern on a rigid disk is caused by the periodic vortex structure which occurs when the laminar boundary layer becomes unstable. It exists only over a small rotational Reynolds-number range, typically 1.9×10^5–2.8×10^5 in previous investigations (Dorfman 1963). Below this range the boundary layer on the disk is fully laminar, while above it a fully turbulent condition prevails. In contrast the flow-induced waves on a flexible surface can first appear in a laminar or a turbulent flow (figures 4 and 5). They are also observed in the flat-plate geometry as well as on a rotating disk (Hansen *et al.* 1979; Hansen *et al.* 1980). This flow-induced wave phenomenon occurs when the perturbation wall pressure imposed by the fluid at the solid–liquid interface in response to an infinitesimal deformation of this interface exceeds the elastic restoring forces in the compliant material (Hansen & Hunston 1974). In general the phenomenon studied in the present work has nothing to do with the initial stages of the laminar-to-turbulent transition on a disk.

The influence of liquid viscosity on the onset flow velocity for the wave structure is probably due to its influence on the boundary-layer thickness near the outer rim of the disk. In qualitative terms the boundary-layer thickness on the disk increases with viscosity at a constant rotational speed, and the perturbation pressure associated with a wave structure in the compliant surface decreases correspondingly. Thus the rotational speed necessary to sustain a deformation in the compliant surface becomes larger as viscosity is increased, as observed in figure 8.

This viscosity effect on onset may be quantified for laminar flow on a disk, subject to a number of simplifying assumptions. (i) The fluid velocity above a wave crest of infinitesimal amplitude is normal to the crest. (ii) The propagation velocity of the wave crest is negligibly small compared to the freestream fluid velocity. (iii) The perturbation pressure generated by the fluid at a point on the solid–fluid interface due to an infinitesimal deformation of this interface is the same for flat-plate and rotating-disk boundary layers when the local wall shear stress is the same in the two cases. The first two of these assumptions are consistent with all past experiments conducted on the flow-induced surface-wave phenomenon (Hansen *et al.* 1979) as well as the results of the present work. The third assumption is equivalent to neglecting the influence of streamline curvature on the perturbation pressure imposed by the fluid. It is supported by the author's previous comparative studies of the onset condition for the surface waves on disks and flat plates (Hansen *et al.* 1980). The measured freestream fluid velocity at the onset point, as well as the corresponding wall shear stress computed from well-known formulas for flat-plate and rotating-disk boundary layers, agreed to within approximately 10 %. These comparisons were made for equivalent fluid and compliant-surface properties, and the freestream fluid velocity was defined in terms of the reference frame rotating with the disk. In these circumstances an analysis of the wall-pressure perturbation conducted for the flat-plate geometry can be coupled with the shear-stress expressions for the rotating disk to predict the dependence of the perturbation pressure on liquid viscosity and other relevant parameters. For the case of sinusoidal variation of wave height y with distance x in the flow direction, Bordner (1978) has shown that

$$p = -\rho\epsilon\left(\frac{\lambda}{\nu}\right)^{\frac{4}{3}}(u_*)^{\frac{10}{3}}(0.776)\cos\left(\frac{x}{\lambda}-\frac{\pi}{6}\right) \tag{4}$$

for
$$y = \epsilon \cos \frac{x}{\lambda}, \tag{5}$$
$$\frac{\epsilon}{\lambda} \ll l. \tag{6}$$

Here λ and ϵ are the characteristic wavelength and maximum wave amplitude respectively, ρ and ν the liquid density and kinematic viscosity, and u_* the friction velocity, defined as the square root of the ratio of wall shear stress to liquid density. Dorfman (1963) has shown that the wall shear stress (τ_ϕ) in the circumferential direction at the radial extremity of a disk of radius R is

$$\tau_\phi = 0.616 \rho R \nu^{\frac{1}{2}} \omega^{\frac{3}{2}}, \tag{7}$$

where ω is the rotational speed of the disk in rad/s. The combination of (4) and (7) yields the following expression for p:

$$p = -0.346 \epsilon \lambda^{\frac{4}{3}} R^{\frac{5}{3}} \nu^{-\frac{1}{2}} \omega^{\frac{5}{2}} \cos\left(\frac{x}{\lambda} - \frac{\pi}{6}\right). \tag{8}$$

The magnitude of p is thus proportional to the quotient $(\omega^5/\nu)^{\frac{1}{2}}$, other parameters being held constant. For a given disk radius and shear modulus of the compliant material, therefore, the minimum rotational speed necessary to sustain the wave structure should vary as $\nu^{\frac{1}{5}}$. This is in fact the case in the two smaller-disk experiments where the onset is in the laminar regime (experiments 2 and 5). The ratio $\omega/\nu^{\frac{1}{5}}$ is 2218 and 2151 rad/s for the two experiments respectively, where ν has been normalized by ν_W in both cases. This variation is well within the experimental uncertainty for the onset-flow and kinematic-viscosity measurements.

When the complexity of the experimental test system is increased by using the polymer solution, quantitative models become very difficult to formulate. Nevertheless, a number of qualitative observations are in order. Although the polymer solutions are non-Newtonian and have a slightly higher shear viscosity than water at low shear rates, the differences are only about 10 %. In light of the results discussed above, this difference in shear viscosity is too small to produce any significant change in the behaviour of the coated disk. It is reasonable to assume, therefore, that the differences in behaviour between the disks in water and in polymer solution arise from viscoelastic effects involving more than the shear viscosity. The exact nature of these effects is unclear. The photographic studies, however, suggest that the polymer solution alters the turbulent-flow field and thereby changes the nature of the wave structure. This altered structure has a more regular appearance, which might be expected to produce a smaller increase in drag than that obtained for the wave structure present in water. It is this feature, plus the fact that the normal drag-reducing mechanisms may also be present, that may explain the very large reductions in drag seen for the coated disk in the polymer solution. Further theoretical work is needed, however, to establish a more quantitative picture of viscoelastic effects.

5. Conclusions

Liquid properties have a significant influence on the flow-generated deformations of a homogeneous, isotropic surface. The onset flow velocity for the wave structure increases with increasing liquid viscosity, and the geometry of the waves is affected, the major change being an increase in wavelength for high-viscosity fluids. In all cases, the skin friction is affected. The drag of the coated disk is greater than that of the solid disk when the wave structure is present.

If the viscosity is sufficiently large, the onset of the wave structure occurs in the laminar-flow regime. In this range the experimentally observed onset-velocity–viscosity relationship is correctly predicted by a straightforward analytical treatment.

When viscoelasticity is introduced by using very dilute high-molecular-weight polymer solutions, the onset speed of the wave structure is unchanged. At higher flow velocities, however, the wave structure has a more orderly appearance than it does in a Newtonian fluid under similar conditions. Since the drag-increasing effect of wave structure is substantially greater in most cases than the drag-reducing effect of the polymer solution, the torque coefficient for the coated disk in the polymer is usually greater than that for the solid disk in water. The 'smoothing' effect of the polymer solution on the wave structure plus possible contributions from the normal drag-reducing mechanisms in the polymer solutions, however, produce a much lower drag for the coated disk in the polymer solution than for the same coated disk in water.

The authors gratefully acknowledge the financial support of the Naval Research Laboratory and the assistance of Mr Glenn E. Ford in conducting the experiments reported herein. Certain commercial materials and equipment are identified in this paper in order to specify adequately the experimental procedure. In no case does such identification imply recommendation or endorsement by the U.S. Government, nor does it imply necessarily the best available for the purpose.

REFERENCES

BORDNER, G. L. 1978 Nonlinear analysis of laminar boundary layer flow over a periodic wavy surface. *Phys. Fluids* **21**, 1471.

BROWN, R. N. 1977 Turbulent pressure spectrum measurements of a compliant surface. In *Turbulence in Liquids: Proc. 4th Biennial Symp. on Turbulence in Liquids*, p. 210.

DORFMAN, L. A. 1963 *Hydrodynamic Resistance and the Heat Loss of Rotating Solids.* Oliver and Boyd.

GREGORY, N., STUART, J. T. & WALKER, W. S. 1955 On the stability of three-dimensional boundary layers with application to the flow due to a rotating disk. *Phil. Trans. R. Soc. Lond.* **A248**, 155.

HANSEN, R. J. & HUNSTON, D. L. 1974 An experimental study of turbulent flows over a compliant surface. *J. Sound Vib.* **34**, 297.

HANSEN, R. J. & HUNSTON, D. L. 1976 Further observations on flow-generated surface waves in compliant surfaces. *J. Sound Vib.* **46**, 593.

HANSEN, R. J., HUNSTON, D. L., NI, C. C. & REISCHMAN, M. M. 1980 An experimental study of flow-generated waves on a flexible surface. *J. Sound Vib.* **68**, 317.

HANSEN, R. J., HUNSTON, D. L., NI, C. C., REISCHMAN, M. M. & HOYT, J. W. 1979 Hydrodynamic drag and surface deformations generated by liquid flows over flexible surfaces. In *Progress in Aeronautics and Astronautics: Viscous Flow Drag Reduction* **72**, 439.

LITTLE, R. C., HANSEN, R. J., HUNSTON, D. L., KIM, O. K., PATTERSON, R. L. & TING, R. Y. 1975 The drag reduction phenomenon: observed characteristics, improved agents, and proposed mechanisms. *Ind. Engng Chem. Fund.* **14**, 283.

METZNER, A. B. & METZNER, A. P. 1970 Stress levels in rapid extensional flows of polymeric fluids. *Rheol. Acta* **9**, 174.

TING, R. Y. & HUNSTON, D. L. 1977 Polymeric additives as flow regulators. *Ind. Engng Chem.: Prod. R. & D.* **16**, 129.